

Journal of Materials Chemistry A

Accepted Manuscript



This is an *Accepted Manuscript*, which has been through the Royal Society of Chemistry peer review process and has been accepted for publication.

Accepted Manuscripts are published online shortly after acceptance, before technical editing, formatting and proof reading. Using this free service, authors can make their results available to the community, in citable form, before we publish the edited article. We will replace this *Accepted Manuscript* with the edited and formatted *Advance Article* as soon as it is available.

You can find more information about *Accepted Manuscripts* in the [Information for Authors](#).

Please note that technical editing may introduce minor changes to the text and/or graphics, which may alter content. The journal's standard [Terms & Conditions](#) and the [Ethical guidelines](#) still apply. In no event shall the Royal Society of Chemistry be held responsible for any errors or omissions in this *Accepted Manuscript* or any consequences arising from the use of any information it contains.

Cite this: DOI: 10.1039/c0xx00000x

www.rsc.org/xxxxxx

ARTICLE TYPE

Photovoltaic Behaviour of Lead Methylammonium Triiodide Perovskite Solar Cells Down to 80 K

Hua Zhang,^{a,‡} Xianfeng Qiao,^{a,‡} Yan Shen,^a Thomas Moehl,^b Shaik Zakeeruddin,^b Michael Graetzel^b and Mingkui Wang^{a,*}

⁵ Received (in XXX, XXX) Xth XXXXXXXXXX 20XX, Accepted Xth XXXXXXXXXX 20XX

DOI: 10.1039/b000000x

We have tested the photovoltaic metrics of CH₃NH₃PbI₃ perovskite solar cells over a wide temperature ranging from 80-360 K. Our investigation reveals that the open-circuit voltage reaches a maximum value at about 200 K close to the phase transition from tetragonal to the orthorhombic phase. The photocurrent is remarkably stable down to 240 K but drops precipitously upon approaching - and below the phase transition temperature, implying inefficient charge carrier generation from the orthorhombic perovskite structure. The impedance spectroscopy measurement clearly shows organic cation ionic motion with in the bulk of CH₃NH₃PbI₃ after a phase transition. We propose a plausible mechanism for these phenomena and discuss implications for photovoltage generation and charge carrier transport in CH₃NH₃PbI₃ perovskite solar cells.

Introduction

Photovoltaic devices based on thin film technologies are desirable to offer sustainable, renewable green energy with reduced materials and fabrication cost.¹ In particular thin film solar cells fabricated by solution-processing based on semiconductor quantum dots^{2,3}, organic polymers^{4,5}, or dye-sensitized nanocrystals⁶⁻⁸ have received considerable attention, showing promising 7~13% solar to electric power conversion efficiencies (PCE). Recently, a new class of highly efficient solid-state hybrid lead halide-based perovskite photovoltaics has emerged, achieving a certified PCE of 20.1%.⁹⁻¹²

Hybrid lead halide perovskites such as methylammonium lead triiodide (CH₃NH₃PbI₃) exhibit strong solar light harvesting via a direct optical transition extending to 800 nm, whose cross section is an order of magnitude higher than that of typical ruthenium dyes.^{10,13} Apart from light absorption, another noteworthy feature of CH₃NH₃PbI₃ (MAPbI₃, CH₃NH₃⁺ being abbreviated as MA thereafter) is its ambipolar semiconducting property enabling it to transport photo-generated electrons and holes to their respective collector electrodes.¹⁴⁻¹⁷ In this respect, hybrid lead methylammonium triiodide based perovskite solar cells are different from dye-sensitized solar cells (DSSCs) that need a semi-conductive mesoporous scaffold to support the light harvester and collect the photo-generated electrons. By contrast perovskite solar cells can function without the mesoporous TiO₂ scaffold.¹⁷⁻¹⁹ Likewise, perovskite solar cells without hole transport material (HTM) system have shown substantial PCEs.^{13,20} However, information on the effect of temperature on the photovoltaic behaviour of the new perovskite solar cells is still lacking. Here we investigate the photovoltaic parameters of MAPbI₃ solar cell from 360 K down to 80 K and propose a mechanism which

accounts for our observations.

Experimental Section

Device Preparation

Fluorine-doped tin oxide (F:SnO₂) coated glass (Pilkington TEC 15, 15 Ω/square) was patterned by etching with Zn powder and 2 M HCl diluted in milliQ water. The etched substrate was then cleaned with 2% hellmanex diluted in milliQ water, rinsed with milliQ water, and ethanol and dried with clean dry air. The substrate was underwent in a UV-O₃ chamber for 30 minutes prior to spray pyrolysis at 500 °C using 40 mL of a titanium di-isopropoxidebis(acetylacetonate) solution (75% in 2-propanol, Sigma-Aldrich) diluted in ethanol (1:39, v/v) and oxygen as carrier gas, and sintered on a hot plate for 1 h at 500 °C. The TiO₂ compact layer thickness determined by scanning electron microscopy (SEM) was ~30 nm. Porous TiO₂ films of 200 nm thick were deposited onto compact layer covered substrates by spin coating at 5000 rpm during 30 s using a TiO₂ paste (Dyesol 30NRD, 30 nm average particle size) diluted in anhydrous ethanol (1:3, weight ratio). After drying at 80 °C, the TiO₂ layers were heated to 470 °C for 15 min.

The mesoporous TiO₂ films were infiltrated with PbI₂ by spin-coating a PbI₂ solution in DMF (462 mg mL⁻¹) that was kept at 70 °C. After drying, the films were dipped in a solution of CH₃NH₃I₃ in 2-propanol (10 mg mL⁻¹) for 30 s and rinsed with 2-propanol and dried at 70 °C for 30 min. After drying, the CH₃NH₃PbI₃-adsorbed films were covered with HTM layer by spin coating at 4000 rpm for 30 s in a dry box. The HTM recipe was prepared by dissolving 72.3 mg of (2,2',7,7'-tetrakis(N,N-di-p-methoxyphenylamine)-9,9-spiro-bifluorene) (*spiro*-MeOTAD), 28.8 μL of 4-tert-butylpyridine, and 17.5 μL of a stock solution of 520 mg mL⁻¹ lithium bis-(trifluoromethylsulfonyl)imide in

acetonitrile in 1 mL of chlorobenzene. Finally, 65 nm of gold was thermally evaporated in the vacuum chamber on top of the device to form the electrode contacts. The device fabrication was carried out under controlled atmospheric conditions and a humidity of <1.0 ppm.

Samples Characterization

A solar simulator with a Xenon light source (450 W, Oriel, model 9119) and an AM 1.5G filter (Oriel, model 91192) was used to give an irradiance of 100 mW cm^{-2} at the surface of the solar cell. The current-voltage characteristics of the cell were obtained by applying an external potential bias to the cell and measuring the photocurrent generated under these conditions on a Keithley model 2400 digital source meter (USA). The J-V curves were obtained in reverse (from the V_{OC} to the J_{SC}) scan at a scan rate of 20 mV s^{-1} . A similar data-acquisition system was used to control the photon-to-current response (internal quantum efficiency, IQE) measurements. A white-light bias of 10 % solar intensity was applied onto the sample during the IPCE measurements, which employed monochromatic light modulated at 10 Hz. The temperature was controlled from 360 K down to 80 K within ± 0.5 K by a temperature controller (Oxford, optistat DN-TM). Impedance spectra (IS) were performed with an Autolab Frequency Analyzer setup consisting of the Autolab PGSTAT 30 (Eco Chemie B.V., Utrecht, The Netherlands) and the Frequency Response Analyzer module. The measurements were performed at V_{OC} in the frequency range 0.01 Hz~1 MHz with oscillation potential amplitudes of 30 mV. The $\text{CH}_3\text{NH}_3\text{PbI}_3$ covered electrode was connected to the working electrode. The Au electrodes were connected to the auxiliary electrode and the reference electrode. The impedance measurements were carried out under open circuit potential (via tuning the bias light intensity with white LED light radiation). The obtained impedance spectra were fitted with the Z-view software (v2.8b, Scribner Associates Inc.). Low temperature differential scanning calorimetry (DSC) was performed on a SDT 2010 thermal analyser swept at the rate of $10^\circ\text{C}/\text{min}$ from -170°C to 0°C under nitrogen and in heating mode.

Results and Discussion

Figure 1a presents a scheme of our cell configuration featuring a compact and nanocrystalline layer of TiO_2 deposited on TCO coated glass infiltrated with MAPbI_3 which is covered by *spiro*-OMeTAD and a gold back contact. Figure 1b shows a cross-sectional SEM image of the fabricated device. Within the device structure one distinguishes the thin compact TiO_2 layer on top of the FTO, followed by the mesoscopic TiO_2 scaffold with a thickness of ~ 200 nm. The latter was infiltrated with MAPbI_3 using the previously described sequential deposition method.¹¹ The mean TiO_2 particle diameter was 30 nm with a porosity of 69% determined by BET. On top of the $\text{TiO}_2/\text{MAPbI}_3$ nanocomposite there is a MAPbI_3 capping layer forming a smooth contact with the hole conductor. The spiro-MeOTAD layer exhibits a dense structure with a total thickness of 100 nm.

The photocurrent-voltage curve of the perovskite solar cell device measured under 100 mW cm^{-2} AM 1.5G simulated irradiation at room temperature is shown in Figure 2a. In order to reduce the influence from the direct adsorption of FTO glass and oxide semiconductors on the photovoltaic data, a sheet of YC-

AR130 (an anti-reflecting UV cut-off film, Japan) was attached to each cell surface for J-V and IPCE measurements. The best device displayed a short-circuit current density (J_{SC}) of 22.19 mA cm^{-2} , a fill factor (FF) of 0.72, an open-circuit voltage (V_{OC}) of 1.01 V, achieving a PCE of 16.1% for a reverse scan. The voltage scan rate in J-V measurement was kept at 20 mV per step with a delay time of 1 ms. The device showed a lower PCE of 12.4% when measured in a forward scan direction. We ascribe the large hysteretic behaviour to the $\text{CH}_3\text{NH}_3\text{PbI}_3$ film with a small grain size of less than 150 nm by using the fabrication procedure as described in experiment section.¹¹ The small grain size of $\text{CH}_3\text{NH}_3\text{PbI}_3$ would result in an increase of defect concentration which has been experimentally verified to be responsible for hysteretic behaviour.²¹ The hysteresis effect could be largely retarded in those devices using perovskite film with millimeter-scale crystalline grains formed with hot-casting method by Nie *et al* for instance.²² The IQE reaches a broad maximum at around 500 nm remaining at a level over 80% up to 750 nm (Figure 2b). The appearance of plateau at such a high IPCE level indicates that the MAPbI_3 efficiently harvests visible light, converting it with near unit quantum yield to electric current.

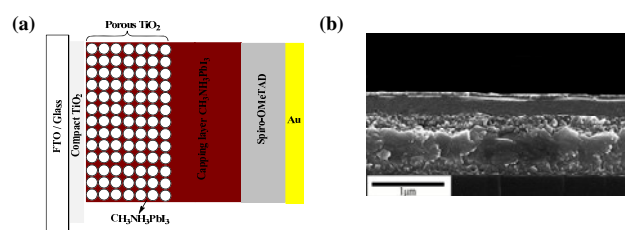


Fig. 1 Schematic device structure and (b) a cross-sectional SEM image of perovskite solar cells used in this study.

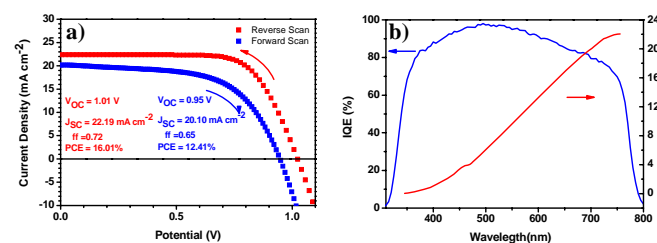


Fig. 2 (a) Photocurrent density-voltage (J-V) characteristics with reverse and forward scan directions under AM 1.5 illumination (100 mW cm^{-2}) at room temperature. Cells were tested at 20 mV per step with a delay time of 0.001 s. and (b) Internal quantum efficiency action spectra (left ordinate) and the integrated photon-to-current response (J_{SC}) on a solar spectrum at AM 1.5 versus wavelength of the perovskite solar cell in this study. A sheet of YC-AR130 (an anti-reflecting UV cut-off film, Japan) was attached to each cell surface for J-V and IPCE measurements. Cell active area tested (with a mask): 0.2505 cm^2 .

We measured the photocurrent density vs. voltage (J-V) curves at different temperatures in the range between 80 and 360 K. The photovoltaic metrics derived from this analysis are summarized in Table 1. The V_{OC} shows a maximum value of 1.15 V at about 200 K, indicating that a thermo-dynamic equilibrium state between charge recombination and generation is reached at this

temperature. The J_{SC} is remarkably stable down to 240 K but drops precipitously upon approaching-and below the Curie temperature (~ 160 K, Figure S1), implying inefficient charge carrier extraction in the paraelectric and ferroelectric domain. The highest J_{SC} obtained was 22.7 mA cm^{-2} at 280 K. The increase of photocurrent in the range of 200-300 K was accompanied by an augmentation of the fill factor compensating the decrease in the V_{OC} . It is noted that the photovoltaic parameters (V_{OC} , J_{SC} , FF) of

Table 1 Summary of the photovoltaic parameters of the lead methylammonium triiodide perovskite solar cells at temperature between 80 K and 360 K.

T [K]	Scan direction ^{a)}	V_{oc} [V]	J_{sc} [mA cm^{-2}]	FF	PCE [%] ^{b)}
80	RS	0.87 ± 0.01	0.38 ± 0.02	0.18 ± 0.02	0.06 (0.055)
	FS	0.84 ± 0.02	0.35 ± 0.01	0.18 ± 0.01	0.05 (0.049)
100	RS	0.88 ± 0.01	0.48 ± 0.03	0.17 ± 0.01	0.07 (0.067)
	FS	0.86 ± 0.02	0.44 ± 0.01	0.16 ± 0.01	0.06 (0.056)
120	RS	0.89 ± 0.02	0.62 ± 0.04	0.16 ± 0.02	0.09 (0.086)
	FS	0.88 ± 0.01	0.58 ± 0.05	0.16 ± 0.01	0.06 (0.055)
140	RS	0.94 ± 0.02	1.13 ± 0.05	0.16 ± 0.01	0.17 (0.165)
	FS	0.91 ± 0.01	1.05 ± 0.04	0.15 ± 0.01	0.14 (0.135)
160	RS	1.05 ± 0.01	2.04 ± 0.03	0.17 ± 0.02	0.36 (0.34)
	FS	1.03 ± 0.01	1.96 ± 0.04	0.16 ± 0.01	0.32 (0.31)
180	RS	1.13 ± 0.02	4.38 ± 0.03	0.21 ± 0.01	1.04 (1.02)
	FS	1.11 ± 0.01	4.29 ± 0.04	0.20 ± 0.01	0.95 (0.94)
200	RS	1.15 ± 0.01	8.10 ± 0.04	0.26 ± 0.01	2.42 (2.38)
	FS	1.10 ± 0.01	7.50 ± 0.03	0.24 ± 0.01	1.98 (1.95)
220	RS	1.14 ± 0.02	13.03 ± 0.05	0.31 ± 0.02	4.60 (4.50)
	FS	1.08 ± 0.01	12.10 ± 0.06	0.26 ± 0.01	3.39 (3.30)
240	RS	1.12 ± 0.02	19.98 ± 0.06	0.39 ± 0.03	8.72 (8.65)
	FS	1.05 ± 0.01	17.50 ± 0.05	0.30 ± 0.01	5.51 (5.45)
260	RS	1.10 ± 0.02	21.90 ± 0.05	0.50 ± 0.02	12.05 (12.00)
	FS	0.98 ± 0.01	20.15 ± 0.06	0.44 ± 0.01	8.69 (8.65)
280	RS	1.07 ± 0.01	22.70 ± 0.06	0.63 ± 0.03	15.30 (15.18)
	FS	0.96 ± 0.01	20.55 ± 0.06	0.56 ± 0.01	11.04 (11.00)
300	RS	1.01 ± 0.03	22.19 ± 0.05	0.72 ± 0.01	16.13 (16.10)
	FS	0.95 ± 0.01	20.10 ± 0.06	0.65 ± 0.01	12.41 (12.35)
320	RS	0.95 ± 0.02	21.24 ± 0.05	0.71 ± 0.01	14.63 (14.55)
	FS	0.88 ± 0.01	19.86 ± 0.04	0.65 ± 0.01	11.36 (11.32)
340	RS	0.90 ± 0.01	19.35 ± 0.05	0.68 ± 0.02	11.84 (11.75)
	FS	0.86 ± 0.01	18.50 ± 0.04	0.60 ± 0.01	9.55 (9.50)
360	RS	0.83 ± 0.02	17.57 ± 0.05	0.64 ± 0.03	9.33 (9.20)
	FS	0.80 ± 0.01	16.60 ± 0.04	0.64 ± 0.01	8.50 (8.46)

a) Scan direction involving reverse scan (RS) and forward scan (FS). b) Average PCEs in brackets.

the perovskite solar cells decrease largely as temperature being higher than 340 K, presumably due to an accelerated interfacial recombination among the charge selective contacts/MAPbI₃. As a

result, the overall power conversion efficiency reaches a maximum value of 16.1% at about 300 K. The mobility of electrons in the nanocrystalline TiO₂ scaffold and that of holes in the *spiro*-MeoTAD increases with temperature since their transport involves thermally assisted carrier trapping and de-trapping and inter-molecular hopping, respectively.²³ This improves the carrier collection efficiency resulting in the observed increase in J_{SC} with temperature, which is a common feature for bulk heterojunction solar cells.²⁴ However, the J_{SC} and FF dropped to very small values below the phase transition temperature of 161 K where the MAPbI₃ turns ferroelectric.²⁸ For example, at 80 K, their respective J_{SC} and FF values are 0.38 mA cm^{-2} and 0.18. A plot of the logarithm of J_{SC} as a function of $1/T$ showed two different regimes with a break point at about 160 K (Figure S1 in supporting information) indicating a smaller activation energy for photocurrent generation in the orthorhombic (ferroelectric) MAPbI₃ phase compared to the tetragonal one. The role of ferroelectric domain formation in inducing this distinct behaviour remains to be elucidated.

The temperature dependence of the V_{OC} in the MAPbI₃-based device deviates from the linear behaviour observed as a rule for organic and inorganic solar cells.^{24,25} Further insight in this unusual behaviour was gained by applying impedance spectroscopy (IS). The IS measurements were performed at open circuit under illumination with an LED array emitting white light at about 1 sun intensity. Figures 3, S2, and S3 show the Nyquist plots for the perovskite solar cell at different temperatures. Three elements can be distinguished when the impedance measurement is performed at 300-360 K as shown in Figure 3a. The first arc in the high frequency regime (100 kHz~600 kHz) is assigned to the charge exchange process at the *spiro*-MeOTAD/Au interface¹⁶ while the semicircle in the intermediate frequency region (50 Hz~100 kHz) corresponds to charge carrier recombination, *i.e.* interfacial recombination of the electrons in the TiO₂ with holes in MAPbI₃, or electrons in MAPbI₃ with holes in *spiro*-MeOTAD.^{16,26,27} The charge carrier density and recombination rate determine the dark current and - along with the rate of photo-generation of carriers - the V_{OC} . The feature at very low frequencies represents a process with long relaxation time and is so far still under discussion in the literatures^{16,26-28} but has been attributed to a ferroelectric effect or an ionic movement inside the perovskite (see below the qualitative observation on the low frequency element).³¹

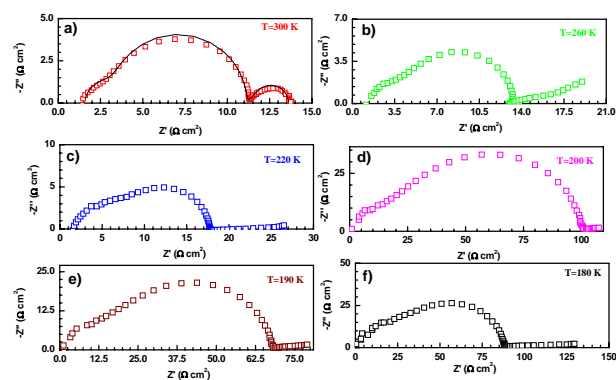


Fig. 3 Impedance spectrum measured under illumination by 100% solar light intensity at open circuit at different temperature. a) 300 K, b) 260 K, c) 220 K, d) 200 K, e) 190K, and f) 180 K.

As mentioned above the semicircle in the intermediate frequency region relates to the interfacial charge recombination which determines the device V_{OC} . Therefore, we suggest using an equivalent circuit consistent of 3 lumped RC-circuit in series in Figure S3 to fit the impedance data. R represents the interfacial charge transfer resistance, while C indicates the capacitance. Considering the device architecture, the second-arc in the middle frequency region for this device can be assigned to the charge recombination at the MAPbI₃/TiO₂ interface.^{32,33} Figure S4 shows the interfacial charge recombination resistance (R_{ct}) obtained from the curve fitting. As the temperature decreases from 360 K to 220 K, R_{ct} increases first slowly then sharply. It shows the highest value at 200 K when the tetragonal phase is present. This is also reflected in the highest V_{OC} (1.15 V) of the perovskite solar cell device at this temperature. Upon further lowering the temperature the interfacial charge recombination resistance shows a dip most probably related to the phase transition at 161 K before increasing further.

The charge recombination lifetime τ at different temperatures was determined by the formula $\tau = R_{ct} \cdot C$ (where R_{ct} is the recombination resistance and C is the associated capacitance) and presented in Figure 4a as a function of temperature (or the inverse of the temperature). Clearly the recombination lifetime τ decreases with increasing temperature supporting our simplified approach for the impedance analysis. The logarithm of the recombination lifetime shows two different slopes with increasing temperature (Figure 4a), which reflects the corresponding behaviour of the V_{OC} in the same temperature range, being from 80 to 120 K, and from 140 to 220 K (see Table 1). The reduced V_{OC} at lower temperature is due to the lower charge density and/or collection efficiency as reflected by the lower J_{SC} .

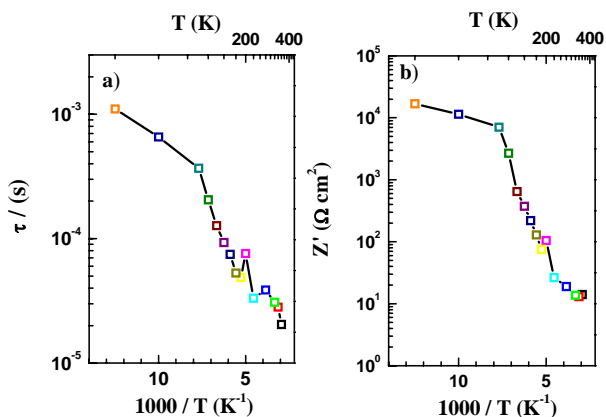


Fig. 4 The a) calculated charge recombination lifetime τ_c and b) real part impedance (Z') as a function of $1000/T$ for the perovskite solar cell examined in this study.

As mentioned above a Warburg-like diffusion impedance was observed in the low frequency range between 0.01 and 50 Hz. It is ascribed to ionic transport or polarisation effect (ferroelectric effect) inside the lattice of the perovskite.^{16,26-28} The frequency

dependent resistance increases with decreasing temperature as shown in Figure 3 and Figure S2 due to slowing down of the ionic transport or the polarisation in the perovskite solar cell.²⁶ Figure 4b presents the real part of the impedance (Z') at 0.1 Hz as a function of reciprocal absolute temperature. In Figure 4b one can observe that the change in the Z' is small for the temperature ranging from 80 to 120 K. For temperatures higher than ~ 120 K, Z' drops significantly. The resistance versus T^{-1} plot provides an indication of increasing conduction with temperature (i.e. negative temperature coefficient of resistance behaviour for typical semiconductor) when the temperature is lower than 200 K. Table 1 also compares the photovoltaic parameters of this device obtained from different scan direction under various temperature. It is interesting to the hysteresis effect becomes weaker when the temperature decreases below than 180K, which might be caused by the phase change and the ionic movements within MAPbI₃. The origin of hysteresis effect is still widely discussed in literatures and its understanding goes beyond the scope of this manuscript.^[34-37]

At equal carrier generation rate, a longer carrier lifetime entails a higher output photovoltage for DSSCs and other organic photovoltaics.^{27,29} The opposite trend is observed within the 80-200 K temperature range reflecting a reduction in the carrier generation rate with decreasing temperature, which is accompanied by a concomitant drop in J_{SC} . Figure S5 presents differential scanning calorimetry measurements of CH₃NH₃PbI₃, showing a distinct peak at 161 K matching well the phase transition temperature. Figure S6 presents the temperature dependence of the real part of the dielectric constant of the perovskite solar cell taken at 0.1 Hz. It shows a discontinuity of ϵ' at around 161 K where the tetragonal-I to orthorhombic II phase transition takes place. The results are in good agreement with previous literature findings.^{30,38} The MA ions are fully disordered in the cubic and tetragonal I phase, i.e., at temperature above 200 K, while they are partially in the tetragonal II phase between 161~200 K. In the orthorhombic phase below 161 K the MA ions are completely ordered and the cations take a fixed position in the lattice.³¹ A similar effect has also been observed in metal-organic framework compounds, such as [NH₄][Zn(HCOO)₃]³⁹ and the [(CH₃)₂NH₂][M(II)(HCOO)₃] series.^{40,41} As shown in Figure 4b, the activation energy E_a for the charge carrier movement was calculated to be about 0.012 eV in the temperature range of 80-160 K and 0.155 eV in the range of 160-200 K using the Arrhenius relation, respectively. This implies that the conductivity of CH₃NH₃PbI₃ in the orthorhombic phase exceeds values extrapolated from the tetragonal one. However, as noted above, the photocurrent and fill factor are very small in the low temperature regime, the photo-generated carrier density in the perovskite solar cell at 80-160 K being several orders of magnitude lower than that at 360 K. Whether this behaviour is caused by the ferroelectric character of the orthorhombic phase needs further investigation. Another possible reason for the small photo-generated charge carrier density at low temperature is the incomplete dissociation of Wannier excitons in the bulk of CH₃NH₃PbI₃ or at the interface with the electron and hole selective contact. The binding energy for excitons in CH₃NH₃PbI₃ is about 19 meV⁴², imposing an energy barrier that strongly reduces their degree of dissociation into free carriers with decreasing temperature.⁴³ Furthermore the band gap of both

TiO₂ and CH₃NH₃PbI₃ increases with decreasing temperature according to $E_g(T) = E_g(0) - (\alpha T^2)/(T + \beta)$ where α [eV/K] and β [K] are material constants, $E_g(0)$ is the energy gap at the temperature $T = 0$ K.⁴⁴ This could affect the band alignment and hence the driving force for exciton dissociation at their interface at lower temperature.

Conclusions

In conclusion, we have investigated the temperature dependence for CH₃NH₃PbI₃ based perovskite solar cell. The photovoltaic metrics were found to be strongly affected by the phase transition from the tetragonal to the orthorhombic phase. The device J_{SC} is very low in the low temperature and presents a drastic increase after the phase transition at 160 K. The device V_{OC} displays a unique nonmonotonic dependence on temperature, achieving to the maximum value of 1.15 V at around 200 K. The impedance investigation reveals that recombination lifetime increases as temperature decreasing, indicating incomplete dissociation of excitons in the low temperature. Organic cation ionic motion with in the bulk of CH₃NH₃PbI₃ is, for the first time, observed with impedance spectroscopy technique after a phase transition. The ionic transport behaviour in impedance study reveals that the movement of cation ions in CH₃NH₃PbI₃ plays important role on device photovoltaic performance. Further investigations are presently carried out to provide a deeper understanding for this intriguing behaviour.

Acknowledgement:

Financial support from the NSFC (21173091, 2110357, and 21161160445) is gratefully acknowledged. The authors thank the Analytical and Testing Centre at the HUST for performing characterization of various samples. MG and TM thank the European Research Council (ERC) for an Advanced Research Grant (No. 247404) funded under the “CE-Mesolight” project.

Notes and references

^a Michael Grätzel Center for Mesoscopic Solar Cells, Wuhan National Laboratory for Optoelectronics, Huazhong University of Science and Technology, Luoyu Road 1037, Wuhan, 430074, P. R. China; E-mail: mingkui.wang@mail.hust.edu.cn

^b Laboratoire de Photonique et Interfaces, Institut des Sciences et Ingénierie Chimique, Ecole Polytechnique Fédérale de Lausanne, CH-1015 Lausanne, Switzerland

† Electronic Supplementary Information (ESI) available: [short-circuit current density as a function of temperature, impedance measurement, and differential scanning calorimetry measurement]. See DOI: 10.1039/b000000x/

‡ These authors contributed equally.

- M. Grätzel, R. Janssen, D. Mitzi, D. B.; E. Sargent, *Nature* **2012**, 488, 304-312.
- A. Ip, S. Thon, S. Hoogland, O. Voznyy, D. Zhitomirsky, R. Debnath, L. Levina, L. Rollny, G. Carey, A. Fischer, K. Kemp, et al., *Nat. Nanotechnol.* **2012**, 7, 577-582.
- Z. Ning, D. Zhitomirsky, V. Adinolfi, B. Sutherland, J. Xu, O. Voznyy, P. Maraghechi, X. Lan, S. Hoogland, Y. Ren, *Adv. Mater.* **2013**, 25, 1719-1723.
- R. Service, *Science* **2011**, 332, 293-293.
- J. You, J. Dou, K. Yoshimura, T. Kato, K. Ohya, T. Moriarty, K. Emery, C. Chen, J. Gao, G. Li, *Nat. Commun.* **2013**, 4, 1446.

- A. Yella, H. Lee, H. Tsao, C. Yi, A. Chandiran, M. Nazeeruddin, E. Diau, C. Yeh, S. Zakeeruddin, M. Grätzel, *Science* **2011**, 334, 629-634.
- L. Han, A. Islam, H. Chen, C. Malapaka, B. Chiranjeevi, S. Zhang, X. Yang, M. Yanagida, *Energy Environ. Sci.* **2012**, 5, 6057-6060.
- I. Chung, B. Lee, J. He, P. Chang, M. Kanatzidis, *Nature* **2012**, 485, 486-489.
- A. Kojima, K. Teshima, Y. Shirai, T. Miyasaka, *J. Am. Chem. Soc.* **2009**, 131, 6050-6051.
- X. Xu, S. Li, H. Zhang, Y. Shen, S. Zakeeruddin, M. Grätzel, Y. Cheng, M. Wang, *ACS Nano*, **2015**, 9, 1782-1787.
- J. Burschka, N. Pellet, S. Moon, R. Humphry-Baker, P. Gao, M. Nazeeruddin, M. Grätzel, *Nature* **2013**, 499, 316-319.
- www.nrel.gov/ncpv/images/efficiency_chart.jpg.
- G. Alemu, J. Li, J. Cui, X. Xu, B. Zhang, K. Cao, Y. Shen, Y. Cheng, M. Wang, *J. Mater. Chem. A* **2015**, DOI: 10.1039/C4TA06126H.
- J. Heo, S. Im, H. Noh, T. Mandal, C. Lim, J. Chang, Y. Lee, H. Kim, A. Sarkar, M. Nazeeruddin, M. Grätzel, S. Seok, *Nat. Photonics* **2013**, 7, 486-491.
- E. Crossland, N. Noel, V. Sivaram, T. Leijtens, J. Alexander-Webber, H. Snaith, *Nature* **2013**, 495, 215-219.
- H. Kim, I. Mora-Sero, V. Gonzalez-Pedro, F. Fabregat-Santiago, E. Juarez-Perez, N. Park, J. Bisquert, *Nat. Commun.* **2013**, 4, 2242.
- M. Lee, J. Teuscher, T. Miyasaka, T. Murakami, H. Snaith, *Science* **2012**, 338, 643-647.
- J. Ball, M. Lee, A. Hey, H. Snaith, *Energy Environ. Sci.* **2013**, 6, 1739-1743.
- M. Liu, M. Johnston, H. Snaith, *Nature* **2013**, 501, 395-398.
- X. Xu, H. Zhang, K. Cao, J. Cui, J. Lu, X. Zeng, Y. Shen, M. Wang, *ChemSusChem*, **2014**, 7, 3088-3094.
- H. Snaith, A. Abate, J. Ball, G. Eperon, T. Leijtens, N. Noel, S. Stranks, J. Wang, K. Wojciechowski, W. Zhang, *J. Phys. Chem. Lett.* **2014**, 5, 1511-1515.
- W. Nie, H. Tsai, R. Asadpour, J. Blancon, A. Neukirch, G. Gupta, J. Crochet, M. Chhowalla, S. Tretiak, M. Alam, H. Wang, A. Mohite, *Science* **2015**, 347, 522-525.
- P. Blom, M. Vissenberg, *Mater. Sci. Eng., R.* **2000**, 27, 53-94.
- E. Katz, D. Faiman, S. Tuladhar, J. Kroon, M. Wienk, T. Fromherz, F. Padinger, C. Brabec, N. Sariciftci, *J. Appl. Phys.* **2001**, 90, 5343.
- S. Hegedus, W. Shafarman, *Prog. Photovoltaics*. **2004**, 12, 155-176.
- E. Barsoukov, J. Macdonald, *Impedance Spectroscopy Theory, Experiment, and Applications*, 2005, John Wiley & Sons, Inc., Hoboken, New Jersey.
- N. Hahn, S. Hoang, J. Self, C. Mullins, *ACS Nano*, **2012**, 6, 7712-7722.
- W. Tress, N. Marinova, T. Moehl, S. Zakeeruddin, M. Nazeeruddin, M. Grätzel, *M. Energy Environ. Sci.*, **2015**, DOI: 10.1039/C4EE03664F
- M. Wang, S. Plogmaker, R. Humphry-Baker, P. Pechy, H. Rensmo, S. Zakeeruddin, M. Grätzel, *ChemSusChem*, **2012**, 5, 181-187.
- A. Poglitsch, D. Weber, *J. Chem. Phys.* **1987**, 87, 6373-6378.
- Z. Xiao, Y. Yuan, Y. Shao, Q. Wang, Q. Dong, C. Bi, P. Sharma, A. Gruverman, J. Huang, *Nat. Mater.* **2015**, 14, 193-198.
- A. Dualeh, T. Moehl, N. Tétreault, J. Teucher, P. Gao, M. Nazeeruddin, M. Grätzel, *ACS Nano* **2014**, 8, 362-373.
- X. Xu, Z. Liu, Z. Zuo, M. Zhang, Z. Zhao, Y. Shen, H. Zhou, Q. Chen, Y. Yang, M. Wang, *Nano Lett.* **2015**, DOI: 10.1021/nl504701y.
- E. Juarez-Perez, R. Sanchez, L. Badia, G. Garcia-Belmonte, Y. Kang, I. Mora-Sero, J. Bisquert, *J. Phys. Chem. Lett.* **2014**, 5, 2390-2394.
- W. Tress, N. Marinova, T. Moehl, S. Zakeeruddin, M. Nazeeruddin, M. Grätzel, *Energy Environ. Sci.*, **2015**, 8, 995-1004.
- B. O'Regan, P. Barnes, X. Li, C. Law, E. Palomares, J. Marin-Belouqui, *J. Am. Chem. Soc.*, **2015**, DOI: 10.1021/jacs.5b00761.
- X. Xu, Z. Liu, Z. Zuo, M. Zhang, Z. Zhao, Y. Shen, H. Zhou, Q. Chen, Y. Yang, M. Wang, *Nano Lett.*, **2015**, DOI: 10.1021/nl504701y.
- N. Onoda-Yamamuro, T. Matsuo, H. Suga, *J. Phys. Chem. Solids*. **1992**, 53, 935-939.
- G. Xu, X. Ma, L. Zhang, Z. Wang, S. Gao, *J. Am. Chem. Soc.* **2010**, 132, 9588-9590.

-
- 40 Z. Wang, B. Zhang, T. Otsuka, K. Inoue, H. Kobayashi, M. Kurmoo, *Dalton Trans.* **2004**, 2209-2216.
- 41 X. Wang, L. Gan, S. Zhang, S. Gao, *Inorg. Chem.* **2004**, 43, 4615-4625.
- 5 42 T. Sum, N. Mathews, *Energy Environ. Sci.*, **2014**, 7, 2518-2534.
- 43 T. Clarke, J. Durrant, *Chem. Rev.*, **2010**, 110, 6736-6767.
- 44 Y. Varshni, *Physica.* **1967**, 34, 149.

Graphical Abstract:

Photovoltaic Behaviour of Lead Methylammonium Triiodide

Perovskite Solar Cells Down to 80 K

Hua Zhang, Xianfeng Qiao, Yan Shen, Thomas Moehl, Shaik M. Zakeeruddin,
Michael Graetzel and Mingkui Wang

Organic cation ionic motion with in the bulk of $\text{CH}_3\text{NH}_3\text{PbI}_3$ becomes visible with impedance spectroscopy technique after a phase transition.

